Structural, electronic and photoluminescence properties of Eu^{3+}-doped CaYAlO$_4$ obtained by using citric acid complexes as precursors

R.V. Perrella [a], C.S. Nascimento Júnior [b], M.S. Góes [c], E. Pecoraro [d], M.A. Schiavon [a], C.O. Paiva-Santos [d], H. Lima [e], M.A. Couto dos Santos [e], S.J.L. Ribeiro [d], J.L. Ferrari [a],*

[a] Grupo de Pesquisa em Química de Materiais − (GPQM), Departamento de Ciências Naturais, Universidade Federal de São João del Rei (UFSJ), Campus Dom Bosco, Praça Dom Helvécio, 74, 36301-160, São João del Rei, MG, Brazil
[b] Laboratório de Química Teórica e Computacional − (LQTC), Departamento de Ciências Naturais, Universidade Federal de São João del Rei (UFSJ), Campus Dom Bosco, Praça Dom Helvécio, 74, 36301-160, São João del Rei, MG, Brazil
[c] Universidade Federal da Integração Latino-Americana (UNILA), Av. Tancredo Neves, 6731 − Bloco 4, Cx P. 2044, CEP: 85867-970, Foz do Iguaçu, PR, Brazil
[d] Instituto de Química, UNESP, P.O. Box 355, 14800-970, Araraquara, SP, Brazil
[e] Departamento de Física, Universidade Federal de Sergipe, 49100-000, São Cristóvão, SE, Brazil

ARTICLE INFO

ABSTRACT

The search for new materials that meet the current technological demands for photonic applications, make the Rare Earth ions embedded in inorganic oxides as excellent candidates for several technological devices. This work presents the synthesis of Eu^{3+}-doped CaYAlO$_4$ using citric acid as ligand to form a complex precursor. The methodology used has big draw due to its easy handling and low cost of the materials. The thermal analysis of viscous solutions was evaluated and the obtained compounds show the formation of a polycrystalline tetragonal phase. Rietveld refinement was used to understand the structural and the cell parameters of the crystalline phase as a function of temperature of heat-treatment. Crystallite size and microstrain were determined and were shown to have a direct relationship with the temperature of the heat-treatment. The band-gap of the CaYAlO$_4$ doped with 1 and 10 mol % of Eu^{3+} showed values close to 4.30 eV, resulting in their transparency in the visible region between 330 and 750 nm. Besides the intense photoluminescence from Eu^{3+}, a study was conducted to evaluate the possible position of the Eu^{3+} in the CaYAlO$_4$ as host lattice. Lifetime of the emission decay from Eu^{3+} excited state $^5D_0$ show that CaYAlO$_4$ is a good host to rare earth ions, once it can avoid clustering of these ions in concentration as high as 10 mol%. The predictions of the sublevels of the $^7F_1$ crystal field level are discussed through the method of equivalent nearest neighbours (MENN). The intensity parameters (Ω_λ, $\lambda = 2$ and 4) are reproduced with physically reasonable values of average polarizabilities. The set of charge factors used in both calculations are in good agreement with the charge of the europium ion described by the Batista-Longo improved model (BLIM). The quantum efficiencies of the materials were calculated based on Judd-Ofelt theory. Based on the results obtained in this work, the materials have potential use in photonic devices such as lasers and solid state imaging devices in the red region of electromagnetic spectrum.

© 2016 Elsevier B.V. All rights reserved.

1. Introduction

Materials doped with Rare Earth ions (RE^{3+} and RE^{2+}) have received special attention due to their unique photoluminescent properties, which have potential application in several technological sectors [1–9]. In recent years, the use of materials doped specifically with RE^{3+} in emitting devices, such as Light Emitting Diodes (LEDs) and Organic Light Emitting Diodes (OLEDs), has grown tremendously [10–12]. The advantage of using these type of devices in comparison to fluorescent lamps, is that they are free of mercury vapor, that even in small amounts, is highly toxic for the environment and humans [12,13]. In particular, LEDs have advantages due their high efficiency, low energy consumption, low operating voltage and longer lifespan when compared to

* Corresponding author. Grupo de Pesquisa em Química de Materiais (GPQM), Universidade Federal de São João del Rei, Departamento de Ciências Naturais, Campus Dom Bosco, Praça Dom Helvécio, 74, Fábricas São João Del Rei, MG, Brazil.
E-mail addresses: ferrari@ufsj.edu.br, jeffersonferrari@gmail.com (J.L. Ferrari).

fluorescent lamps [12].

Recently, inorganic oxides doped with RE^{3+} have been used for the development of White Light Emitting Diodes (WLEDs) [13–16]. Usually, WLEDs are composed by a junction of a blue LED chip emitting at 465 nm with a yellow light phosphor emitter ($Y_3Al_5O_{12}:Ce^{3+}$) [13,14]. However, due to lack of red light emitters, this combination shows a poor color reproduction, limiting their application for electronic devices [15]. Another approach used for manufacturing of WLEDs is combining LEDs, with different intensities of blue, green and red emissions excited by a near ultraviolet InGaN chip, which gives rise to the sense of white color [13–15,17]. Nevertheless, the red light emitting phosphor currently used, $Y_2O_2S:Eu^{3+}$, exhibit low chemical and physical stability [13].

An alternative way of solving the problem of chemical and physical instability of the $Y_2O_2S:Eu^{3+}$ is to use aluminates as host matrices for Eu^{3+}. Aluminates are more stable than sulphides and fluorides, and have higher mechanical strength and thermal conductivity [18]. Particularly, the $CaYAlO_4$ has received much attention in recent years [18–20]. It presents a structure similar to K_2NiF_4, with space group of I4/*mmm* [18]. It belongs to the family of compounds with general formula $ABCO_4$, wherein A is a cation from alkaline-earth metals group, B is Y^{3+}, Sc^{3+}, or RE^{3+} and C is a trivalent ion like Al^{3+}, Ga^{3+} or transition metal ion. This crystal structure is composed by perovskite type structures, where Al^{3+} ions occupy sites of octahedral symmetries, while divalent A and trivalent cations B are randomly distributed in sites of C_{4v} symmetry.

In the literature, there are many methods of synthesis reported, like sol–gel process [21], Czochralski crystal growth [22], the chemical solution technique [23] and the uses of cation complexation with citric acid ligands, also known as amorphous citrate process [24–26]. Citric acid is well known for its easy forming of complexes, due to the molecules to form highly stable rings, especially with transition metal cations [27]. Furthermore, this technique has several advantages, such as pH control, homogeneity of the precursor solution, low cost and obtaining metal aluminate solution at low temperatures, when compared with other synthesis routes, such as solid state synthesis [25].

By using the local structure of the luminescent site, crystal field calculations were performed using the method of equivalent nearest neighbours (MENN) [28], in order to discuss the sublevels of the $^7F_1$ level. Intensity parameters (Ω_λ, $\lambda = 2$ and 4), related to the $^5D_0 \rightarrow {}^7F_{2,4}$ transitions, were also predicted through the dynamics coupling mechanism described earlier [29]. Also, the Batista-Longo improved model (BLIM) [30] is used to compare the set of charge factors which enter in the MENN.

Based on that, this work presents the synthesis of $CaYAlO_4$ containing Eu^{3+} in different concentrations, based on the use of citric acid to form complexes precursors. The study of the photoluminescence, electronic and structural properties of these materials were performed and related to the concentration of Eu^{3+} and to the different heat-treatment temperatures.

2. Experimental procedure

$CaYAlO_4$ containing 1, 3, 5, 7 and 10 mol% of Eu^{3+} in powder form were synthesized by use citric acid (Synth-99.5%) to form complexes precursors. This experimental procedure was based on our previous work reported in literature [1] with slight modifications. Stoichiometric amounts of Y_2O_3 (Aldrich − 99.999%), $CaCO_3$ (Dynamic − 99%), $Al(NO_3)_3.9H_2O$ (Synth − 99%) and Eu_2O_3 (Aldrich − 99.999%) were dissolved in acidic aqueous solution. The solutions were standardized based on complexometric titration with EDTA 0.01 mol L^{-1} as titrant. The defined volumes of the solution

containing Eu^{3+} were pipetted into some beakers, to obtain materials doped with different amounts of Eu^{3+}. The follow, a mass corresponding to 5 times the citric acid as a function of number of moles of the metals were dissolved in deionized water and transferred to a beaker containing Ca^{2+}, Y^{3+}, Al^{3+} and Eu^{3+} to obtain the homogenous solution precursor. The complexes solutions were kept under magnetic stirring at 70 °C by 6 h, which leads to an increasing in the solutions viscosities. For each concentration of Eu^{3+}, viscous solutions were obtained. The viscous solutions containing 1, 5 and 10 mol% of Eu^{3+} were submitted to thermogravimetric analysis (TG) and differential thermal analysis (DTA) by using a thermobalance Shimadzu model DTG − 60H, from room temperature up to 1100 °C, with heating rate of 10 °C/min, under air atmosphere. All viscous solutions were dried in an oven at 120 °C for 24 h and then, heat-treated at 900, 1000 and 1100 °C for 5 h. The morphology of the materials obtained after the heat-treatment were analyzed by Scanning Electron Microscopy, SEM (Hitachi TM-3000). The crystalline structure was evaluated by X-ray diffraction (XRD) by a Shimadzu XRD 6000 diffractometer with Cr Kα radiation ($\lambda = 2.2897$ Å) in the range 2θ between 30° and 120°. The microstrain and average crystallite sizes were determined based on diffractograms obtained. The Rietveld refinements [31] were performed using the General Structure Analysis System (GSAS) software with an EXPGUI interface [32]. Parameters of crystallites structure were based on the reference of ICSD 72104 ($CaYAlO_4$), ICSD 63650 ($Al_2Y_4O_9$) and ICSD 86815 (Y_2O_3). The Fourier Transform Infrared Spectroscopy (FTIR) analyses were carried out operating the spectrophotometer Perkin Elmer Spectrum GX. The samples were prepared in the form of transparent pellets diluted into KBr and kept under pressure of around 10 tons during 1 min. The spectra were collected in the region between 4000 and 400 cm^{-1} with 4 cm^{-1} of spectral resolution. The diffuse reflectance spectra were carried out operating the Varian spectrophotometer Cary model 5000 between 250 and 750 nm with 0.2 nm of spectral resolution. Based on diffuse reflectance spectra, electronic structural properties were evaluated. The photoluminescence measurements were performed at room temperature using a spectrofluorometer Shimadzu, Model RF − 5301 PC equipped with a xenon lamp of 150 W. The emission spectra were obtained at 300 K within the range of 550–750 nm under excitation fixed at 394 nm, which corresponds to the electronic transition $^7F_0 \rightarrow {}^5L_6$ of Eu^{3+} [33]. The excitation and emission slits were fixed at 5 and 2 nm, respectively. The measurements of the lifetime of the $^5D_0$ excited state of the Eu^{3+} were performed at 300 K using the spectrofluorometer SPEX Fluorolog F2121 equipped with phosphorimeter and pulsed lamp, with excitation at 394 nm and emission at 620 nm, with excitation and emission slits of 5 and 2 nm, respectively.

3. Results and discussion

The studies of the thermal behavior of the viscous solutions obtained in this work were carried out for samples containing 1, 5 and 10 mol% of Eu^{3+}. The Fig. 1 shows the TG and DTA curves of the viscous solutions. The first thermal event occurs approximately at 107 °C and can be attributed to the dehydration of the solution and also to the loss of uncomplexed citric acid [34]. The loss of mass occurs continuously up to approximately 600 °C followed by an exothermic event above 400 °C, which can be related to decomposition of organic matter in the form of $CO_{(g)}$ and $CO_{2(g)}$. The mass loss continuously indicates that the thermal decomposition is of Type I, in accordance to Courty, et al. [24]. It is known that compounds prepared using citric acid as the complexing agent may present two Types of thermal decomposition, labeled Type I and Type II. The thermal decomposition of Type I is characterized by a
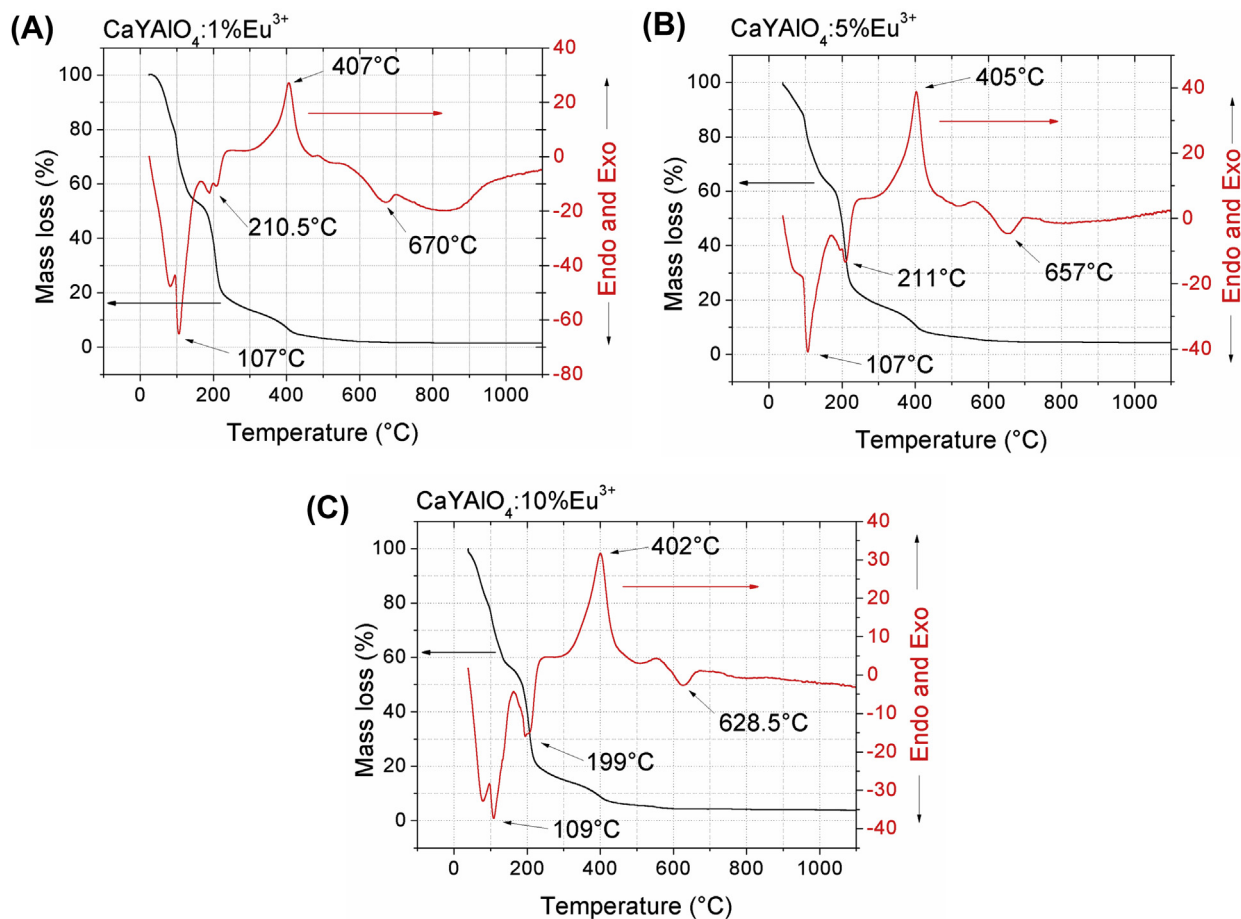
Fig. 1. TG and DTA analysis of the viscous solutions containing Eu^{3+}: (A) 1, (B) 5 and (C) 10 mol% from room temperature up to 1100 °C.

continuous weight loss, whereas Type II breakdown is determined by the formation of an intermediate stage, where the semi-stable complex is decomposed. Thus, the main difference between both types of breakdown is the thermal stability of the obtained metal citrate [24,34]. At temperatures above 628 °C, an endothermic event occurs without any corresponding loss of mass, which indicates the beginning of $CaYAlO_4$ formation. The results show that the temperature of $CaYAlO_4$ formation decreases with the increasing of Eu^{3+} concentration. This suggests that a higher concentration of Eu^{3+} decrease the thermal stability of the complexes, and favors the formation of $CaYAlO_4$.

The FTIR analysis was used to evaluate the presence of the species that can act as suppressors for photoluminescent. The presence of hydroxyl groups can promote the non-radiative process, which cause the deactivation of the excited state of Eu^{3+} by vibrational modes, and reduces the intensity of the photoluminescence.

The Fig. 2 shows the FTIR spectra of citric acid, viscous solutions obtained during the synthesis, and the materials obtained after heat-treatment at 900, 1000 and 1100 °C. The bands of citric acid were identified and assigned as follows: 3292, 3447 and 3497 cm^{-1} — stretching of OeH bonds; at 1749 and 1705 cm^{-1} — stretching of C]O bonds of the COOH groups of citric acid; at 1176 and 1137 cm^{-1} — stretching of CeO [35]. The same bands could be observed in the spectra of viscous solutions, which confirm the presence of citrate unchanged molecules. One can also observe that the increasing in the temperature of the heat-treatment promotes the decreasing of the intensity of the band assigned to the OeH groups, which

suggests the reduction of the concentration of OeH groups, favoring the radiative mechanisms of photoluminescence. However should be noted that even after heat-treatment, bands assigned to the stretching of OeH groups are observed in the systems. The presence of OeH bonds after heat-treatment at high temperatures has been discussed in the works reported by Seco, et al. [36].

The bands between 400 and 812 cm^{-1} are attributed to the metal-oxygen bonding. The band at 810 cm^{-1} is attributed to the stretching of the AleO bonds [37], while the band at 471 cm^{-1} is attributed to stretching of the YeO bonds [38].

The study about crystalline structure and the purity of the materials obtained after heat-treatment were performed using XRD analysis. Fig. 3 shows the XRD diffractograms patterns of the samples doped with 1, 3, 5, 7 and 10 mol% of Eu^{3+} heat-treated at 900, 1000 and 1100 °C for 5 h. The indexed diffraction peaks are in good agreement with the ICSD standard No. 72104. However all the diffractograms present some reflections that are not typical of the $CaYAlO_4$ phase, suggesting the presence of other phases, called secondary or spurious phases.

To confirm and quantify the presence of these secondary phases, Rietveld refinement was carried out in three samples, which are representative of the behavior of the system in study: $CaYAlO_4$ doped with 1, 5 and 10 mol% of Eu^{3+} heat-treated at 1100 °C. Table 1 exhibits the results obtained from the Rietveld refinements. Quantitative analysis by the Rietveld method indicates that the majority phase, with approximately 95% in weight, is $CaYAlO_4$, and the secondary phases are $Al_2Y_4O_9$ and Y_2O_3. We observed that all samples have at least two phases, and only the sample with 5 mol%

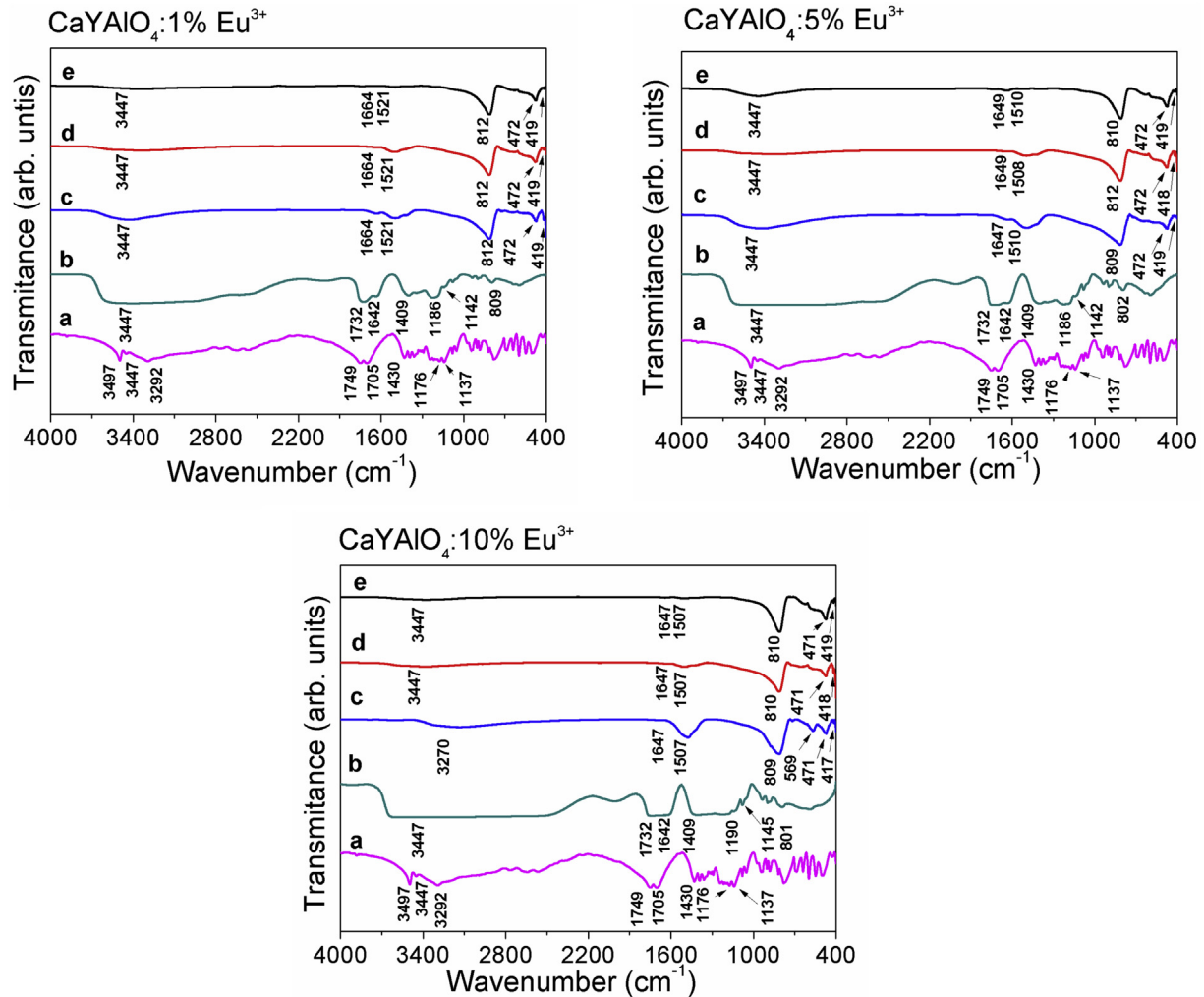**Fig. 2.** FTIR analysis of the (A) citric acid, (B) viscous solutions and the synthesized CaYAlO₄:Eu³⁺ (1, 5 and 10 mol% of Eu³⁺) after heat-treatment at (C) 900, (D) 1000 and (E) 1100 °C during 5 h.

of Eu³⁺ presents the CaYAlO₄, Al₂Y₄O₉ and Y₂O₃ phases.

The values of the parameters cells and volume of major phase are presented in Table 2. The results show good agreement with other values reported in the literature and standard ICSD 72104 (CaYAlO₄) [18,20]. It is possible to observe the increasing in the values of lattice parameters and of the volume, when the concentration of Eu³⁺ in the host changes from 1 to 5 mol%. On the other hand, when the Eu³⁺ concentration is 10 mol%, there is a decrease in these values.

The Fig. 4 shows the crystal structure of CaYAlO₄. The lattice parameters are a = b = 3.6451 Å and c = 11.8743 Å, with space group I4/mmm (D$^{17}_{4h}$). The Y³⁺ and Ca²⁺ are distributed randomly and they occupy the same site of symmetry C_{4v}, keeping a ratio of 1:1. These ions are surrounded by nine oxygen atoms, while the Al³⁺, bonded to six oxygen atoms, forming octahedral structures containing an inversion center (i). The position occupied by the Eu³⁺ into the crystalline structure of CaYAlO₄ is strongly affected by the size of its ionic radius. As a consequence, it is expected that the Eu³⁺ will preferentially occupy the sites of Ca²⁺ and Y³⁺, because the ionic radius of Eu³⁺ (1.206 Å) is very close to the ionic radii of Ca²⁺ (1.26 Å) and Y³⁺ (1.16 Å), and much larger than the radius of Al³⁺ (0.675 Å). The difference between the ionic radii of Eu³⁺ and Ca²⁺/Y³⁺ is around 4%, while the difference between the ionic radii of Eu³⁺ and Al³⁺ is more than 40%. Furthermore, the similar valence

also influences the position occupied by the dopant ions, which causes the Y³⁺ been preferably substituted by Eu³⁺ in the structure of CaYAlO₄. This behavior explains the increasing of the lattice parameters and volume, when the concentration of Eu³⁺ ranges from 1 to 5 mol%. On the other hand, the decreasing in these values when Eu³⁺ is 10 mol%, may be related to Eu³⁺ substituting Ca²⁺. Due to the radius of Eu³⁺ be smaller than the ionic radius of Ca²⁺, it is expected a reduction in the volume of the unit cell, as shown by Rietveld calculations.

In order to evaluate the effect on the concentration of Eu³⁺ as dopant, as well as the thermal treatment temperature, Scherrer's equation (Equation (1)) [39] was used to calculate the average of crystallite size of the materials. The calculation was based on the reflection with higher intensity around 2θ = 50.5°.

$$D_{hkl} = \frac{K\lambda}{\beta \cos\theta} \tag{1}$$

In the Scherrer's equation, D$_{hkl}$ is the average of crystallite size (nm), K (0.89) is the shape factor (which varies from 0.89 for spherical to 0.94 for cubic particles), λ is the wavelength of the radiation of the X-rays used in the experiment (Cr K$_\alpha$ = 2.28970 Å), β is the full width half maximum and θ is the diffraction angle of the most intense peak on the diffractogram. The broadening of the

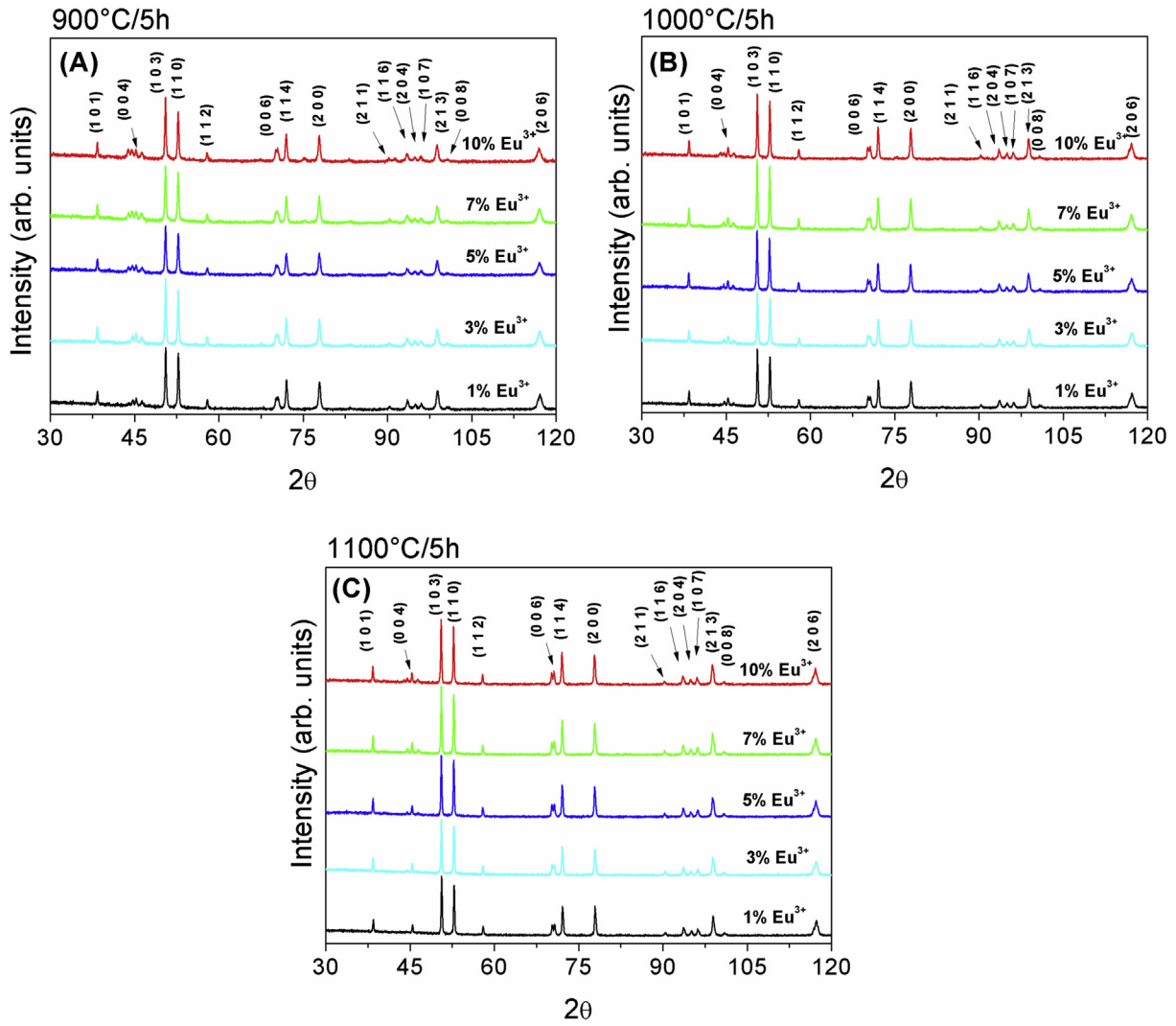**Fig. 3.** X-Ray diffractograms of the samples containing 1, 3, 5, 7 and 10 mol% of Eu^{3+} heat-treated at (A) 900, (B) 1000 and (C) 1100 °C for 5 h.

Table 1
Rietveld agreement indices. * Major phase.

	1 mol% of Eu^{3+}	5 mol% of Eu^{3+}	10 mol% of Eu^{3+}
R indexes			
R_{wp} (%)	7.32	10.25	13.89
R_F^2 (%)	8.89	12.95	27.57
R_{Bragg}(%)*	2.02	2.58	5.80
S	1.04	0.98	0.96
% of Mass			
CaYAlO$_4$	97.772(2)	92.18(7)	96.250(9)
Al$_2$Y$_4$O$_9$	2.2(1)	6.4(2)	3.75(4)
Y$_2$O$_3$	–	1.3(1)	–

Table 2
Results obtained by the Rietveld refinement for CaYAlO$_4$:Eu^{3+} (1, 5 and 10 mol%) heat-treated at 1100 °C for 5 h.

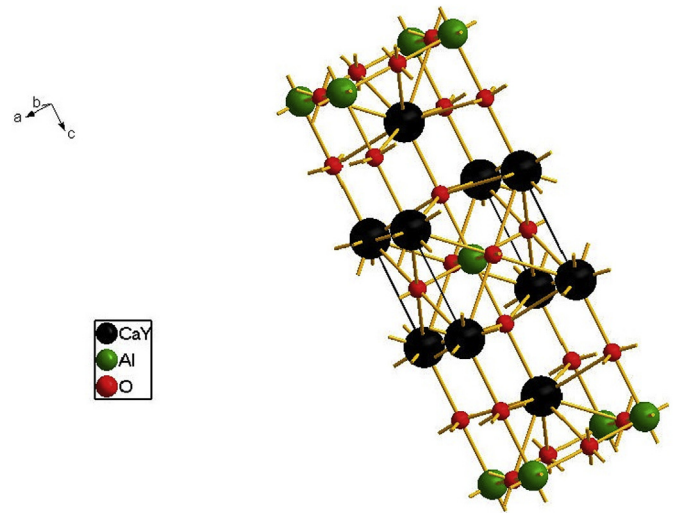| Cell parameters (a = b ≠ c)			
Sample	a (Å)	b (Å)	c (Å)	Volume (Å)
1% Eu^{3+}	3.64532(4)	3.64532(4)	11.8854(1)	157.939(4)
5% Eu^{3+}	3.64778(6)	3.64778(6)	11.8978(2)	158.316(6)
10% Eu^{3+}	3.64639(9)	3.64639(9)	11.8899(4)	158.091(1)

Fig. 4. The unit cell structure of CaYAlO$_4$.

reflection has been corrected taking into account the instrumental

broadening, as shown in Equation (2). The values for instrumental broadening were obtained by analyzing the XRD pattern of crystalline Si.

$$\beta = [(\beta_{\text{measured}})^2 - (\beta_{\text{instrumental}})^2]^{\frac{1}{2}} \qquad (2)$$

Fig. 5(A) summarizes the results of crystallite size obtained by XRD. The results suggest an increasing of the crystallites sizes as a function of thermal treatment temperature. In addition, the increasing in the concentration of Eu^{3+} does not cause a significant variation in the values of crystallite for all the temperatures of the heat-treatment. The microstrain values were determined and the results are shown in Fig. 5(B). The Williamson-Hall [40] method given in Equation (3) was used to calculate these values.

$$\beta\cos\theta = \frac{K\lambda}{D_{hkl}} + 4\varepsilon sen\theta \qquad (3)$$

In this equation, D_{hkl} is the size of the crystallites, K is the shape factor (0.89), λ is the wavelength of the radiation $CrK_\alpha = 2.28970$ Å, β is the value of the Full Width Half the Maximum (FWHM) of the reflection peaks with the instrumental correction, θ is the angle of reflection and ε is the value of microstrain related to crystal imperfections and distortion of strain-induced peak broadening. The Fig. 5(B) shows that the number of defects is reduced with increasing of temperature of the heat-treatment, indicating that the crystallinity is dependent on the temperature. Moreover, these results are in agreement with those obtained in Fig. 3, where the intensity of the diffraction peaks of the secondary phase are reduced, when the temperature change from 900 to 1100 °C, suggesting a reduction in the number of defects of these materials.

Fig. 6 shows the SEM images of the samples treated at 900—1100 °C containing 1, 5 and 10 mol% of Eu^{3+}. It can be seen that the materials are composed of aggregates of small particles with large amount of pores and cracks. It is observed directly the dependence of volume of porous as function of temperature of heat-treatment temperature. As the annealing temperature increases is seen an increase in the amount of pores in the material.

The diffuse reflectance in the UV−Vis region was used to calculate the experimental band-gap value of CaYAlO4 doped with 1 and 10 mol% of Eu^{3+}. The Fig. 7(A) shows the spectrum obtained for these materials. The results show below 330 nm the samples begin to exhibit low reflectance indicating high radiation absorption. This behavior is assigned to the edge absorption, corresponding to the electronic transition from the valence band to the conduction band of CaYAlO4. The matrix of yttrium aluminate and calcium shows optical transparency in the visible region between 330 and 750 nm, making it a candidate for applications in photonic devices.

The values for the band-gap materials were calculated using the Kubelka-Munk model [41], considering the indirect band-gap of the CaYAlO4. The results presented in Fig. 7(B) do not show a significant changing in the band-gap edge with increasing of dopant concentration. The difference of energy band-gap between samples doped with 1 and 10 mol% of Eu^{3+} is in the order of magnitude of the phonon energy of the lattice. Thus, the results suggest that the increasing of Eu^{3+} concentration into the crystalline structure of CaYAlO4, do not cause a significant changing in its energy band-gap.

Taking as starting point the results obtained by the Rietveld refinement, Fig. 4, we calculated the theoretical band-gap value of the CaYAlO4 phase. The energy gap values were obtained at semi empirical PM7 level of theory through solid state calculation [42]. The main result pointed out the band-gap obtained from HOMO-−LUMO orbitals (Fig. 8) was 4.1 eV. To compare the theoretical band-gap values, the Kubelka−Munk method was employed on the reflectance diffuse spectra shown in Fig. 7(B) with band-gap values between 4.23 and 4.33 eV. The results of the theoretical and experimental band-gap values are in good agreement when compared with the experimental one (4.3 eV). These results emphasize the capability of the use of the PM7 semi empirical method for the prediction of physical chemical properties, as well as the usefulness of theoretical calculations for materials modeling.

The Fig. 9 shows the emission spectra of CaYAlO4 containing 1, 3, 5, 7 and 10 mol% of Eu^{3+} for different heat-treatment temperatures. The excitation wavelength was 394 nm, which corresponds to the transition $^7F_0 \rightarrow {}^5L_6$ of Eu^{3+} [33]. All the emissions are intense and assigned to the intraconfigurational $f-f$ transitions of Eu^{3+}, originated from $^5D_0 \rightarrow {}^7F_J$ levels (J = 0, 1, 2, 3 and 4). The most intense emission around 620 nm is attributed to the hypersensitive transition $^5D_0 \rightarrow {}^7F_2$ (0−2). This transition is strongly influenced by the chemical environment of Eu^{3+} in the host lattice. The presence of Eu^{3+} in symmetry with center of inversion, will results in this transition becomes forbidden. In the crystalline structure of CaYAlO4, Y^{3+} and Ca^{2+} are equivalent and are found in crystallographic sites with symmetry C_{4v}, which can be easily occupied by Eu^{3+}, and presents no center of inversion, which promotes high intensity of photoluminescence as shown in Fig. 9. On the other hand the $^5D_0 \rightarrow {}^7F_1$ (0−1) transition is allowed by magnetic dipole mechanism and its intensity is not sensitive to the chemical

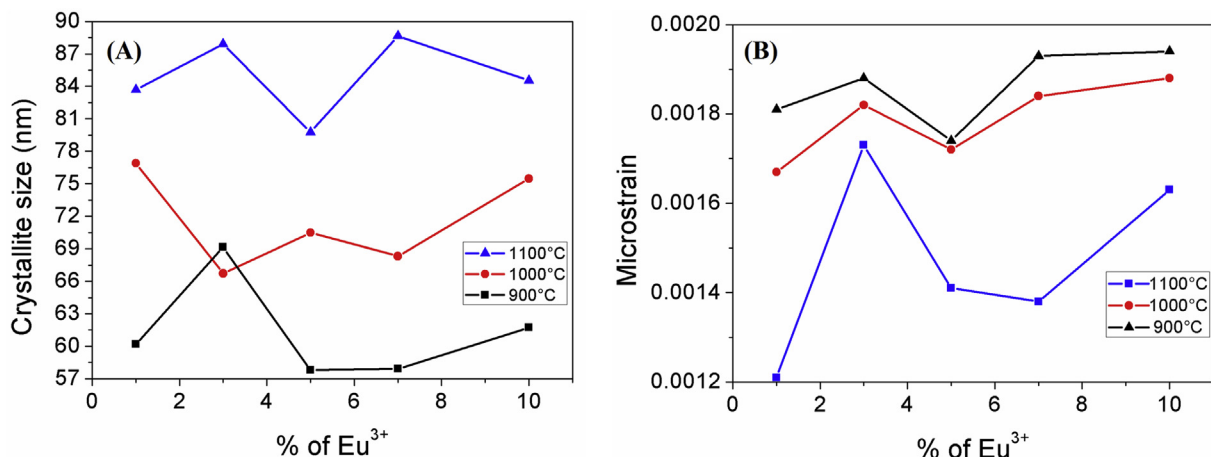**Fig. 5.** (A) Crystallites sizes and (B) microstrain of the materials containing different concentration of Eu^{3+} heat-treated at different temperature.
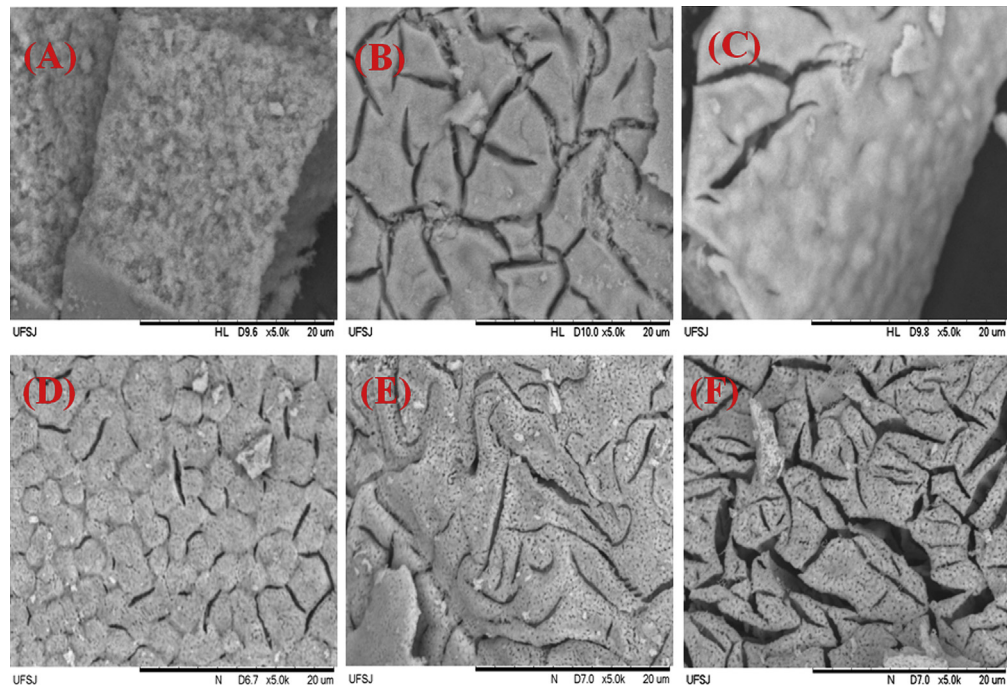
Fig. 6. Images of SEM for $CaYAlO_4$ containing 1, 5 and 10 mol% of Eu^{3+} and heat-treated at (A, B and C) 900 and (D, E and F) 1100 °C for 5 h.
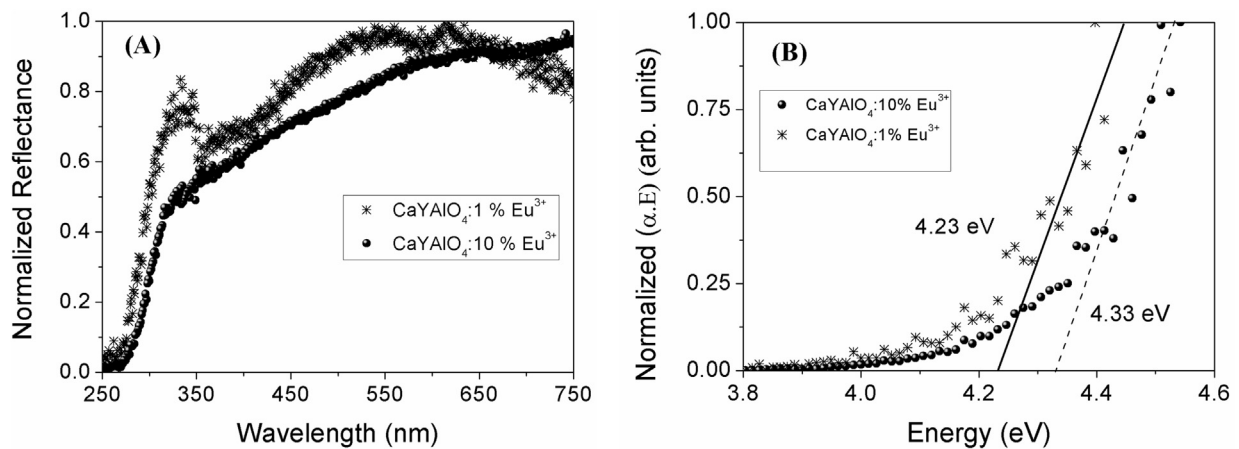

Fig. 7. (A) Diffuse reflectance and (B) band-gap calculated for the material containing 1 and 10 mol% of Eu^{3+} heat-treated at 1100 °C for 5 h.

environment of the Eu^{3+}, therefore it is not changed.

The analysis of the ratio between the areas assigned to these two transitions allows assessing the chemical environment and symmetry of Eu^{3+} in $CaYAlO_4$. The Fig. 10 shows the ratio between the area of the band of hypersensitive transition $^5D_0 \rightarrow {}^7F_2$ (0–2) and the area of the band of transition $^5D_0 \rightarrow {}^7F_1$ (0–1). It shows a trend of increasing the ratio as the annealing temperature decreases. This result indicates that the symmetry of Eu^{3+} is going lower as the temperature of the heat-treatment decreases.

The diffractograms and results for microstrain shown in Figs. 3 and 5(B) corroborate with this conclusion. The samples heat-treated at 900 °C have higher microstrain values and higher intensity of the diffraction peaks are associate to the presence of secondary phases, indicating that the samples have a higher number of defects, when compared to the samples heat-treated at 1000 and 1100 °C. The increase in the number of defects promotes the lowering of symmetry of the Eu^{3+} site, which favors the

emission assigned to the $^5D_0 \rightarrow {}^7F_2$ transition. Furthermore, according to the Fig. 10, the system of $CaYAlO_4$ containing 7 mol% of Eu^{3+} shows the highest intensity emission for the $^5D_0 \rightarrow {}^7F_2$ transition for those samples heat-treated at 900 and 1000 °C.

Lifetime of the emission decay of the excited state $^5D_0$ were obtained for the $CaYAlO_4$ containing 1, 3, 5, 7 e 10 mol% of Eu^{3+} and heat-treated at 900, 1000 and 1100 °C for 5 h. The measurements were performed fixing the excitation at 394 nm and emission at 620 nm. The Fig. 11 shows the decay curve obtained for the sample doped with 1 mol% of Eu^{3+} and submitted to heat-treatment at 1100 °C. The decay curves of the samples annealed at 1000 and 1100 °C were fitted by a first order exponential decay curve, whereas the samples subjected to 900 °C were best fitted by an exponential decay of second order. The average lifetime of the excited state $^5D_0$, 1/e (y = 0.3678), were also calculated and are presented in Table 3. The results indicate that the increasing in the temperature of the heat-treatment favors the Eu^{3+} be found in a

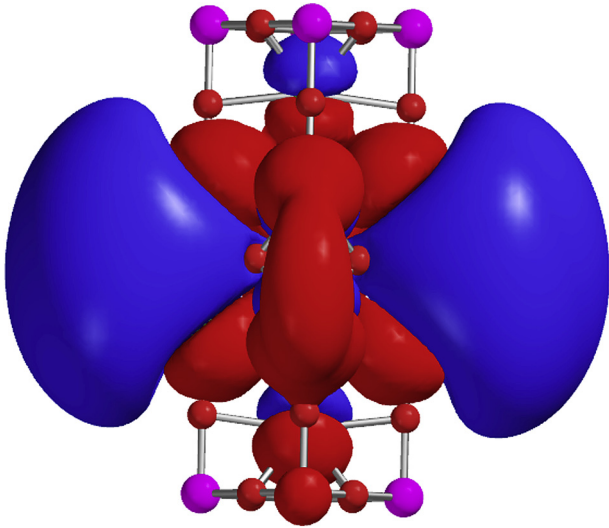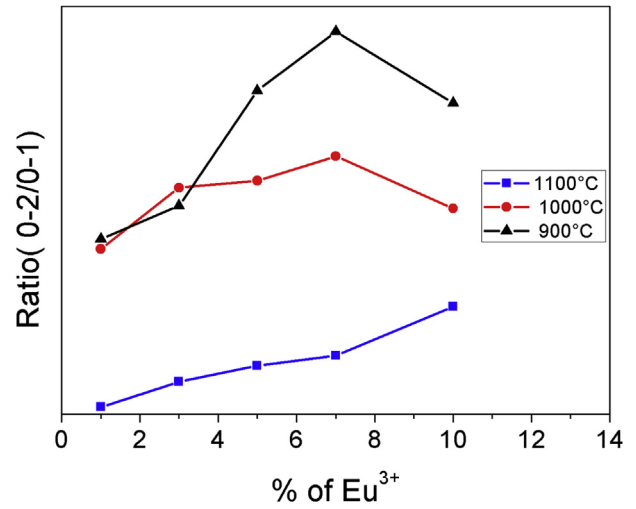**Fig. 8.** HOMO and LUMO frontier orbitals obtained from PM7 solid state calculation for CaYAlO$_4$ unit cell.

Fig. 10. Ratio between the integrated areas corresponding to the $^5D_0 \rightarrow {}^7F_2$ and $D_0 \rightarrow {}^7F_1$ transitions of the Eu^{3+} in CaYAlO$_4$.
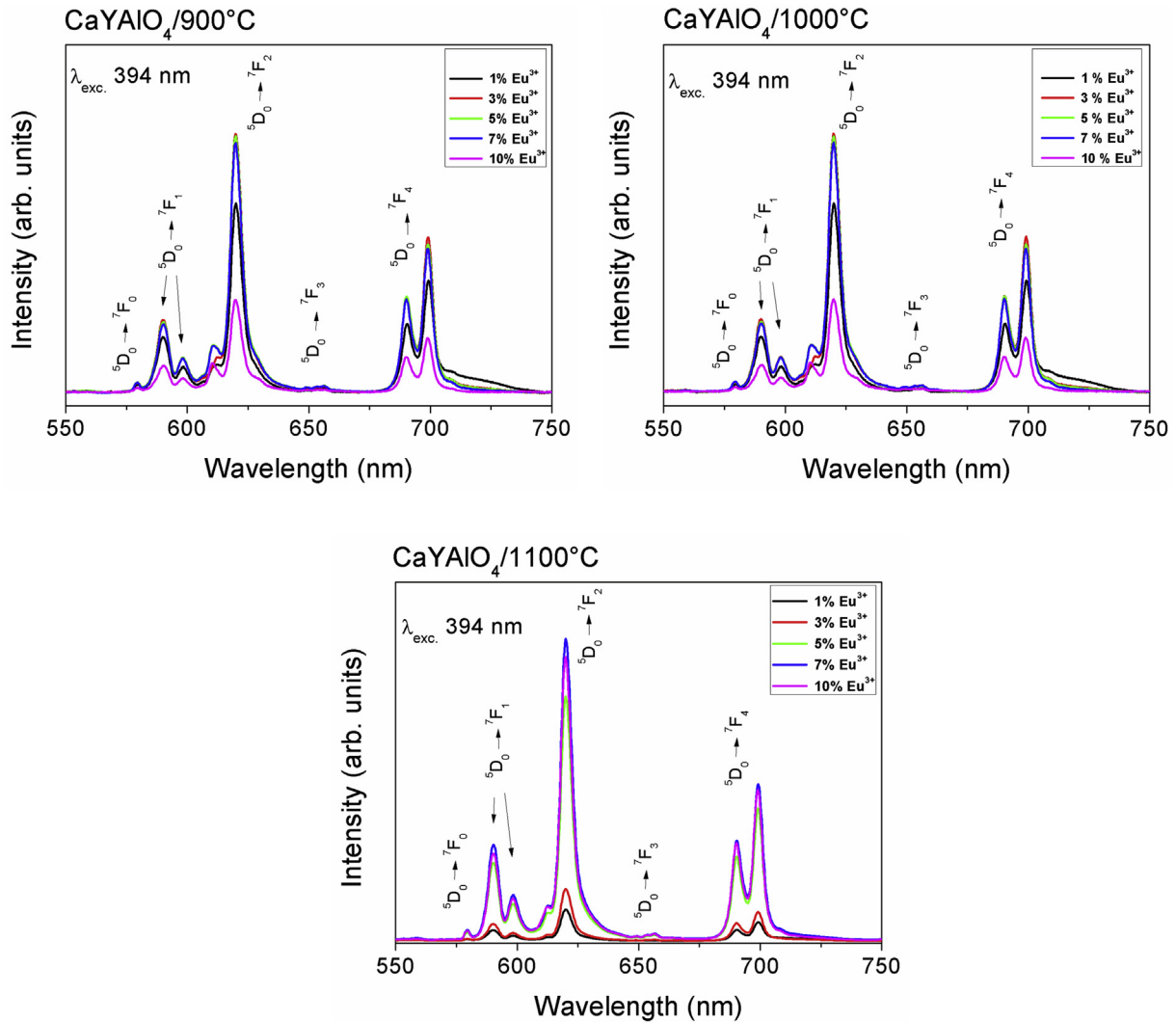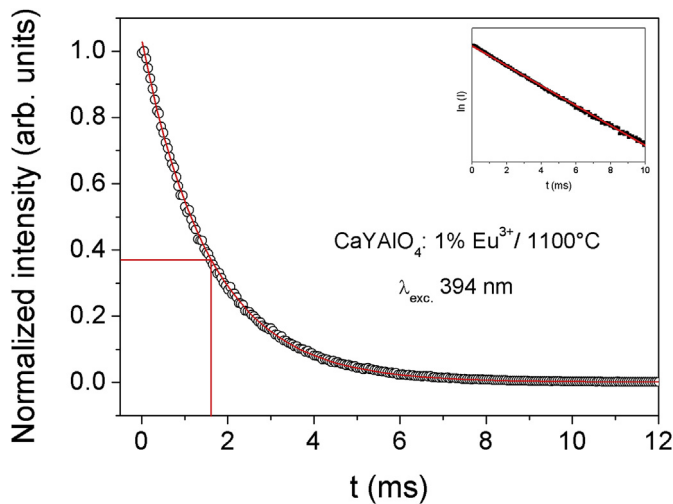

Fig. 9. Emission spectra of the samples containing different concentration of Eu^{3+} and heat-treated at 900, 1000 and 1100 °C for 5 h.

Fig. 11. Lifetime of the emission decay of the excited state $^5D_0$ for the sample containing 1 mol% of Eu^{3+} and heat-treated at 1100 °C for 5 h.

Table 3
Lifetime values of the excited state $^5D_0$ for samples with Eu^{3+} concentration from 1 to 10 mol%. The samples were heat-treated at 900, 1000 and 1100 °C for 5 h.

	Lifetime values (ms)				
	900 °C	1000 °C		1100 °C	
	Dec.	Dec.	1/e	Dec.	1/e
1 mol% Eu^{3+}	1.90	1.62	1.61	1.57	1.63
	0.70				
3 mol% Eu^{3+}	0.56	1.76	1.80	1.69	1.74
	1.73				
5 mol% Eu^{3+}	1.77	2.11	2.15	2.24	2.33
	0.57				
7 mol% Eu^{3+}	1.77	2.08	2.13	2.40	2.48
	0.53				
10 mol% Eu^{3+}	0.53	2.49	2.56	2.74	2.82
	1.69				

Table 4
The spherical coordinates are written following the Eu^{3+} percentage (1/5/10 mol%). For gj and αj follow the choice of equivalent NN. Ω_λ ($\lambda = 2,4$) are in units of $10-20$ cm^2. Both E_0 and $E_{\pm 1}$ and its experimental values have been reproduced.

NN	R(Å)	Θ(°)	φ (°)
O3	2.254/2.259/2.255	0.00/0.00/0.00	0.00/0.00/0.00
4 × O2	2.483/2.485/2.481	132.76/132.78/132.71	45/135/225/315
4 × O1	2.597/2.598/2.599	82.98/83.05/82.84	0/90/180/270
g1/g2/g3	0.371/0.347/0.342		
Σg	3.135/3.115/3.121		
gBLIM	3.43	$E_0 = -75$	$\Omega_2 = 5.35$
αÅ^3	0.683/1.229/0.718	$E_{\pm 1} = 151$	$\Omega_4 = 4.92$

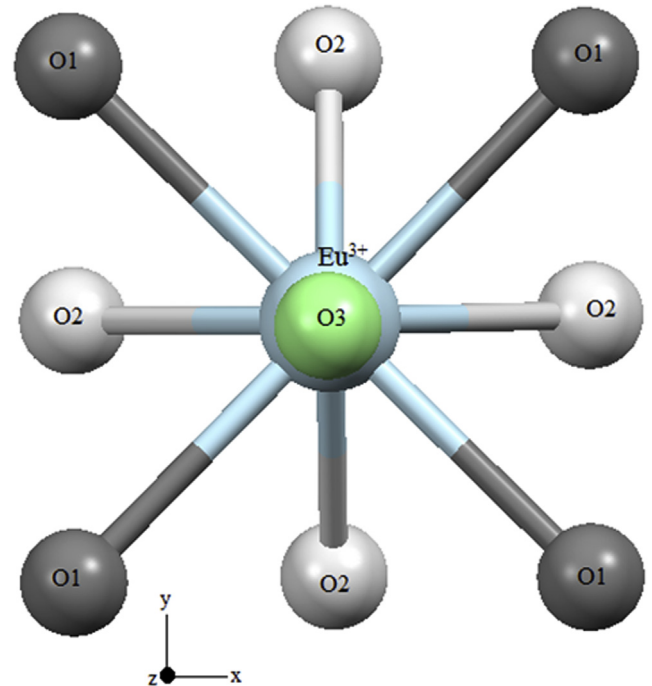**Fig. 12.** Local structure of the Eu^{3+} ion O3 is on the z axis.

site of single symmetry. On the other hand, samples treated at 900 °C show, at least, two distinct sites of symmetry for Eu^{3+}. This result was expected given that, the XRD diffractograms presented in Fig. 3 suggested that for 900 °C the amount of secondary phases present is greater than for those at 1000 and 1100 °C. Starting from 1000 °C the amount of secondary phases is reduced and europium ions are preferentially localized in $CaYAlO_4$ phase. As previously discussed, in the structure of $CaYAlO_4$, Y^{3+} and Ca^{2+} are equivalent regarding the crystallographic symmetry, both belongs to C_{4v} group. Therefore, Eu^{3+} can easily be accommodated in both sites of symmetry, showing lifetime values corresponding to the same symmetry. The results show also an increase in lifetime values as the concentration of Eu^{3+} increases from 1 to 10 mol%. This behavior is observed for samples heat-treated at 1000 and 1100 °C and indicates that the maximum concentration of Eu^{3+}, above which clustering of rare earth ions begins to suppress luminescence and decreases the lifetime, was not reached, yet.

Through the Eu^{3+} ion local structure (Table 4), the crystal field parameters related to the $^7F_1$ level (B^2_q) have been calculated and the energy sublevel positions have been predicted. From Fig. 12, one can note nine oxygen ions as the nearest neighbours (NN). The Eu^{3+} ion local symmetry is C_{4v}, the O3 oxygen being on the C_4 principal axis of symmetry. From the MENN [28] point of view, the number of non-equivalent NN is 3 (c = 3). In Fig. 12, different colours mean different charge factors. This is also true for the polarizabilities. This

means that we cannot have an analytical closed solution, because we have two sublevels (E_0 and $E_{\pm 1}$), with $E_{\pm 1} = -E_0/2$. This means that, with the local neutrality of the luminescent site, one has two equations and three unknowns. In this way, a still phenomenological set of charge factors (g_j, j = 1,2,3) has been used (Table 4). The experimental sublevels of the $^7F_1$ level have been exactly predicted. The difference gBLIM-Σg in percentage is around 10%. Even though BLIM is a model developed to europium complexes, it seems that, in this case, it works quite satisfactorily. For the B^2_0 calculations, only the negative signal of β in the SOM expression was used [28]. This is being used because the ionic radius of the Eu^{3+} ion is smaller than that of the NN.

The experimental intensity parameters have also been exactly predicted with a phenomenological set of polarizabilities (α). The nearest among the NN (O3 in this crystal) had the smaller magnitude of α. This can be an indication that the O3 has the strongest bond and has minor freedom to move. Clearly, the αxR dependence does not follow the same linear behaviour obtained for the gxR behaviour. The σ- and π-types of bonding should play a crucial role in describing the behaviour of the NN ionic polarizabilities. Fig. 13 show that gxR has a decreasing behaviour. The authors suggest that the coordination number of the NN should be taken into account, in order to better discuss such behaviour more properly.
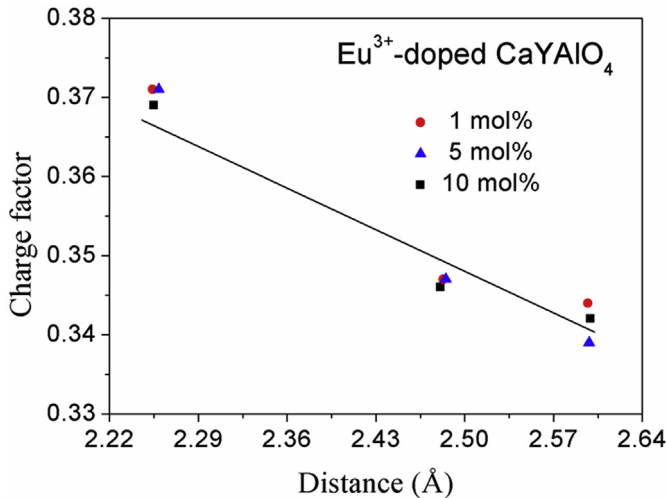
Fig. 13. Charge factor as a function of the EueO distance.

However, in this case, this decreasing behaviour can be interpreted as the Eu − NN wave-functions overlap.

I accordance to the Judd Ofelt theory is possible to calculate the quantum efficiency based on emission spectra and lifetime values. The methodology applied in this work is present in detail by Refs. [43,44]. The results obtained in this work are presented in Tables 5 and 6. It is observed that the quantum efficiency is directly dependent on the Eu^{3+} concentration reaching up to values of 89% of efficiency for samples heat-treated at 1100 °C. The amount of 10 mol% of Eu^{3+} is not sufficient to provoke the photoluminescence suppression.

4. Conclusions

The synthesis methodology used in this study was successful in obtaining $CaYAlO_4$ with different concentrations of Eu^{3+}. This route can also be considered feasible for synthesis of crystalline materials, because it is ease of implementation and presents low cost. The XRD analyzes, together with the results of the Rietveld refinement, showed that the presence of secondary phases and defects are reduced with increasing of the annealing temperature. It was also observed an increase in the crystallite size as the temperature of heat-treatment increases. The presence of secondary phases promotes a distortion of the symmetry around the Eu^{3+}, favoring a higher emission intensity of the $^5D_0 \rightarrow {}^7F_2$ transition for the samples treated at 900 °C. All emissions observed were intense and attributed to electronic transitions of the Eu^{3+} ion ($^5D_0 \rightarrow {}^7F_J$). Crystal field and intensity calculations were used to reproduce the $^7F_1$ Stark levels and splitting, as well as the intensity parameters very satisfactorily. Lifetime of the emission decay from Eu^{3+} excited state $^5D_0$ show that $CaYAlO_4$ is a good host to rare earth ions, once it can avoid clustering of these ions in concentration as high as 10 mol

Table 5
Emission lifetime values, radiative and non-radiative emission rates and quantum efficiencies of the Eu^{3+}-doped $CaYAlO_4$ samples heat-treated at 1000 °C for 4 h.

Samples	τ (ms)	A_{rad} (s^{-1})	A_{nrad} (s^{-1})	η (%)
1% of Eu^{3+}	1.62	370.91	246.37	60.09
3% of Eu^{3+}	1.76	372.08	196.10	65.49
5% of Eu^{3+}	2.11	373.45	100.49	78.80
7% of Eu^{3+}	2.08	371.32	109.45	77.23
10% of Eu^{3+}	2.49	351.18	50.43	87.44

Table 6
Emission lifetime values, radiative and non-radiative emission rates and quantum efficiencies of the Eu^{3+}-doped $CaYAlO_4$ samples heat-treated at 1100 °C for 4 h.

Samples	τ (ms)	A_{rad} (s^{-1})	A_{nrad} (s^{-1})	η (%)
1% of Eu^{3+}	1.57	339.94	297.00	53.37
3% of Eu^{3+}	1.69	324.63	267.08	54.86
5% of Eu^{3+}	2.24	318.08	128.35	71.25
7% of Eu^{3+}	2.40	315.57	101.10	75.74
10% of Eu^{3+}	2.74	325.75	39.21	89.26

%. The quantum efficiency around 90%, when the materials were excited at 394 nm, makes the materials interesting for application as photoluminescence materials in several areas.

References

[1] R.V. Perrella, D.P. dos Santos, G.Y. Poirier, M.S. Góes, S.J.L. Ribeiro, M.A. Schiavon, J.L. Ferrari, Er^{3+}-doped Y_2O_3 obtained by polymeric precursor: synthesis, structure and upconversion emission properties, J. Lumin 149 (2014) 330–340.

[2] J.L. Ferrari, K.O. Lima, E. Pecoraro, R.A.S. Ferreira, L.D. Carlos, R.R. Gonçalves, Color tunability of intense upconversion emission from Er^{3+}−Yb^{3+} co-doped SiO_2−Ta_2O_5 glass ceramic planar waveguides, J. Mater. Chem. 22 (2012) 9901−9908.

[3] B.M. van der Ende, L. Aarts, A. Meijerink, Lanthanide ions as spectral converters for solar cells, Phys. Chem. Chem. Phys. 11 (2009) 11081−11095.

[4] Y. Ledemi, M. Amraoui, J.L. Ferrari, P. Fortin, S.J.L. Ribeiro, Y. Messaddeq, Infrared to visible up-conversion emission in Er^{3+}/Yb^{3+}codopedfluoro−phosphate glass−ceramics, J. Am. Ceram. Soc. 96 (2013) 825−832.

[5] Y. Zhou, Y. Li, Layer-by-layer self-assembly of multilayer films containing DNA and Eu^{3+}: their characteristics and interactions with small molecules, Langmuir 20 (2004) 7208−7214.

[6] J.L. Ferrari, K.O. Lima, L.J.Q. Maia, S.J.L. Ribeiro, R.R. Gonçalves, Structural and spectroscopic properties of luminescent Er^{3+}-doped SiO_2−Ta_2O_5nanocomposites, J. Am. Ceram. Soc. 94 (2011) 1230−1237.

[7] D. Manzani, J.L. Ferrari, F.C. Polachini, Y. Messaddeq, S.J.L. Ribeiro, 1.5 μm and visible up-conversion emissions in Er^{3+}/Yb^{3+} co-doped tellurite glasses and optical fibers for photonic applications, J. Mater. Chem. 22 (2012) 16540−16545.

[8] C.S. Cunha, J.L. Ferrari, D.C. Oliveira, L.J.Q. Maia, A.S.L. Gomes, S.J.L. Ribeiro, R.R.Gonçalves, NIR luminescent Er^{3+}/Yb^{3+} co-doped SiO_2-ZrO_2 nanostructured planar and channel waveguides: optical and structural properties, Mater. Chem. Phys. 136 (2012) 120−129.

[9] J. Gottmann, L. Moiseev, I. Vasilief, D. Wortmann, Manufacturing of Er:ZBLAN ridge waveguides by pulsed laser deposition and ultrafast laser micromachining for green integrated lasers, Mater. Sci. Eng. B 146 (2008) 245−251.

[10] N. Thejokalyani, S.J. Dhoble, Novel approaches for energy efficient solid state lighting by RGBorganic light emitting diodes − a review, Renew. Sust. Energ. Rev. 32 (2014) 448−467.

[11] N. Thejokalyani, S.J. Dhoble, Organic light emitting diodes: energy saving lighting technology − a review, Renew. Sust. Energ. Rev. 16 (2012) 2696−2723.

[12] A. Almeida, B. Santos, B. Paolo, M. Quicheron, Solid state lighting review − potential and challenges in Europe, Renew. Sust. Energ. Rev. 34 (2014) 30−48.

[13] S. Li, X. Wei, K. Deng, X. Tian, Y. Qin, Y. Chen, M. Yin, A new red-emitting phosphor of Eu^{3+}-doped $Sr_2MgMo_xW_{1-x}O_6$ for solid state lighting,, Curr. Appl. Phys. 13 (2013) 1288−1291.

[14] H.S. Jang, H. Yang, S.W. Kim, J.Y. Han, S. Lee, D.Y. Jeon, White light-emitting diodes with excellent color rendering based on organically capped CdSe quantum dots and Sr_3SiO_5:Ce^{3+},Li^+ phosphors, Adv. Mater. 20 (2008) 2696−2702.

[15] X. Li, L. Guan, X. Li, J. Wen, Z. Yang, Luminescent properties of $NaBaPO_4$: Eu^{3+} red-emitting phosphor for white light-emitting diodes, Powder Technol. 200 (2010) 12−15.

[16] R. Xie, N. Hirosaki, M. Mitomo, K. Sakuma, N. Kimura, Wavelength-tunable and thermally stable Li-α-sialon: Eu^{2+}oxynitride phosphors for white light-

emitting diodes, Appl. Phys. Lett. 89 (2006) 241103.

[17] Q. Wang, Z. Ci, G. Zhu, S. Xin, W. Zeng, M. Que, Y. Wang, Multicolor bright Ln^{3+} (Ln = Eu, Dy, Sm) activated tungstate phosphor for multifunctional applications, Opt. Mater. Express 4 (2014) 142–154.

[18] D. Geng, G. Li, M. Shang, C. Peng, Y. Zhang, Z. Cheng, J. Lin, Nanocrystalline $CaYAlO_4$:Tb^{3+}/Eu^{3+} as promising phosphors for full-colorfield emission displays, Dalton Trans. 41 (2012) 3078–3086.

[19] J. Di, X. Xu, C. Xia, D. Li, D. Zhou, Q. Sai, L. Wang, J. Xu, Growth, luminescenceandenergytransferstudiesof Pr3+, Yb3+co-doped $CaYAlO_4$ single crystal, Phys. B 408 (2013) 1–5.

[20] M.S. Kim, J.S. Yu, Synthesis and luminescent properties of nanocrystalline $CaYAlO_4$:Sm^{3+}phosphors, Phys. Status Solidi B 250 (2013) 374–377.

[21] L.K. Kurihara, S.L. Suib, Sol-gel synthesis of ternary metal oxides. 1. synthesis and characterization of $MA1_2O_4$ (M = Mg, Ni, Co, Cu, Fe, Zn, Mn, Cd, Ca, Hg, Sr, and Ba) and $Pb_2A1_2O_5$, Chem. Mater 5 (1993) 609–613.

[22] D. Zhou, X. Xu, X. Chen, H. Zhu, D. Li, J. Di, C. Xia, F. Wu, J. Xu, Crystal growth and spectroscopic properties of Er^{3+}-doped $CaYAlO_4$,Phys, Status Solidi A 209 (2012) 730–735.

[23] J.L. Ferrari, R.L.T. Parreira, A.M. Pires, S.A.M. Lima, M.R. Davolos, A route to obtain Gd_2O_3:Nd^{3+} with different particle size,, Mater. Chem. Phys. 127 (2011) 40–44.

[24] P.H. Courty, H. Ajot, B. Delmon, C.H. Marcilly, Oxydesmixtesou en solution solide sous formetrèsdiviséeobtenus par décompositionthermique de précurseursamorphes, Powder Technol. 7 (1973) 21–38.

[25] J.I. Cosimo, C.R. Apesteguía, Preparation of ternary Cu/Co/Al catalysts by the amorphouscitrate process, J. Catal. 116 (1989) 71–81.

[26] J.L. Ferrari, M.A. Cebim, A.M. Pires, M.A.Couto dos Santos, M.R. Davolos, Y_2O_3: Eu^{3+} (5 mol%) with Ag nanoparticlespreparedbycitrate precursor, J. SolidStateChem. 183 (2010) 2110–2115.

[27] C. Georgi, H. Kern, Preparation of zirconium tungstate (ZrW_2O_8) by the amorphous citrate process, Ceram. Int. 35 (2009) 755–762.

[28] Y.A.R. Oliveira, H. Lima, A.S. Souza, M.A. Couto dos Santos, An alternative description for the interaction between the Eu^{3+} ion and its nearest neighbours, Opt. Mat. 36 (2014) 655–657.

[29] O.L. Malta, M.A. Couto dos Santos, L.C. Thompson, N.K. Ito, Intensity parameters of 4f-4f transitions in theEu(dipivaloylmethanate)31,l0-phenanthroline complex, J. Lumin. 69 (1996) 77–84.

[30] H.J. Batista, R.L. Longo, Improved point-charge model within the INDO/S-CI method for describing the ligand excited states of lanthanide coordination compounds, Int. J. Quantum Chem. 90 (2002) 924–932.

[31] H.M. Rietveld, A profile refinement method for nuclear and magnetic structures, J. Appl. Cryst. 2 (1969) 65–71.

[32] B.H. Toby, EXPGUI, a graphical user interface for GSAS, J. Appl. Cryst. 34 (2001) 210–213.

[33] A. Podhorodecki, G. Zatryb, P. Sitarek, J. Misiewicz, D. Kaczmarek, J. Domaradzki, A. Borkowska, E.L. Prociow, Excitation mechanism of europium ions embedded into TiO_2nanocrystalline matrix, Thin Solid Films 517 (2009) 6331–6333.

[34] R.A. Rocha, E.N.S. Muccillo, Effect of the calcination temperature and dopant content on the physical properties of ceria-gadolinia prepared by the cation complexation technique, Cerâmica 47 (2001) 219–224.

[35] H. Lin, P. Hsu, S. Lin, Theophylline-citric acid co-crystals easily induced byDSC-FTIR microspectroscopy or different storage conditions, Asian J. Pharm. Sci. 8 (2013) 19–27.

[36] A.M. Seco, M.C. Gonçalves, R.M. Almeida, Densification of hybrid silica–titania sol–gel films studied byellipsometry and FTIR, Mater. Sci. Eng. B 76 (2000) 193–199.

[37] P. Tarte, Infra-red spectra of inorganic aluminates and characteristic vibrational frequencies of AlO_4tetrahedra and AlO_6octahedra, Spectrochim. Acta 23A (1967) 2127–2143.

[38] P.Y. Jia, J. Lin, X.M. Han, M. Yu, Pechini sol–gel deposition and luminescence properties of$Y_3Al_{5-x}Ga_xO_{12}$:Ln^{3+} (Ln^{3+}=Eu^{3+}, Ce^{3+}, Tb^{3+}; 0 ≤ x ≤ 5) thin films, Thin Solid Films 483 (2005) 122–129.

[39] A.L. Patterson, The Scherrer formula for X-ray particle size determination, Phys. Rev. 56 (1939) 978–982.

[40] G.K. Williamson, W.H. Hall, X-ray line broadening from filed aluminium and wolfram, Acta Metall. 1 (1953) (1953) 22–31.

[41] P. Kubelka, New contributions to the optics of intensely light-scattering materials. Part I, J. Opt. Soc. Am. 38 (1948) 448–457.

[42] J.D.L. Dutra, M.A.M. Filho, G.B. Rocha, R.O. Freire, A.M. Simas, J.J.P. Stewart, Sparkle/PM7 lanthanide parameters for the modeling of complexes and materials, J. Chem. Theory Comput. 9 (2013) 3333–3341.

[43] R.D.L. Gaspar, E.M. Rodrigues, I.O. Mazali, F.A. Sigoli, Luminescent properties of passivated europium(III)-doped rare earth oxide sub-10 nm nanoparticles, RSC Adv. 3 (2013) 2794–2801.

[44] L.D. Carlos, R.A.S. Ferreira, V.Z. Bermudez, S.J.L. Ribeiro, Lanthanide-containing light-emitting organic–inorganic hybrids: a bet on the future, Adv. Mater 21 (2009) 509–534.